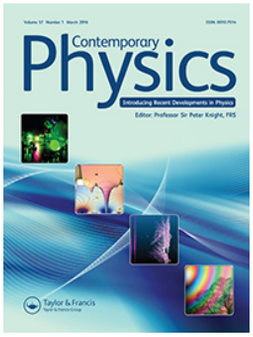

Contemporary Physics

ISSN: 0010-7514 (Print) 1366-5812 (Online) Journal homepage: http://www.tandfonline.com/loi/tcph20

'Twisted' electrons

Hugo Larocque, Ido Kaminer, Vincenzo Grillo, Gerd Leuchs, Miles J. Padgett, Robert W. Boyd, Mordechai Segev & Ebrahim Karimi

To cite this article: Hugo Larocque, Ido Kaminer, Vincenzo Grillo, Gerd Leuchs, Miles J. Padgett, Robert W. Boyd, Mordechai Segev & Ebrahim Karimi (2018): 'Twisted' electrons, Contemporary Physics, DOI: 10.1080/00107514.2017.1418046

To link to this article: https://doi.org/10.1080/00107514.2017.1418046

Published online: 07 Feb 2018.

CONTEMPORARY PHYSICS, 2018
https://doi.org/10.1080/00107514.2017.1418046

Taylor & Francis
Taylor & Francis Group

'Twisted' electrons

Hugo Larocque[a], Ido Kaminer[b], Vincenzo Grillo[c], Gerd Leuchs[a,d,e], Miles J. Padgett[f], Robert W. Boyd[a,d,g], Mordechai Segev[h] and Ebrahim Karimi[a,d]

[a]Department of Physics, University of Ottawa, Ottawa, Canada; [b]Faculty of Electrical Engineering, Technion – Israel Institute of Technology, Haifa, Israel; [c]CNR-Istituto Nanoscienze, Modena, Italy; [d]Max Planck Institut for the Science of Light, Erlangen, Germany; [e]Department of Physics, University of Erlangen-Nuremberg, Erlangen, Germany; [f]School of Physics and Astronomy, University of Glasgow, Glasgow, UK; [g]Institute of Optics, University of Rochester, Rochester, NY, USA; [h]Physics Department and Solid State Institute, Technion-Israel Institute of Technology, Haifa, Israel

ABSTRACT

Electrons have played a significant role in the development of many fields of physics during the last century. The interest surrounding them mostly involved their wave-like features prescribed by the quantum theory. In particular, these features correctly predict the behaviour of electrons in various physical systems including atoms, molecules, solid-state materials, and even in free space. Ten years ago, new breakthroughs were made, arising from the new ability to bestow orbital angular momentum (OAM) to the wave function of electrons. This quantity, in conjunction with the electron's charge, results in an additional magnetic property. Owing to these features, OAM-carrying, or twisted, electrons can effectively interact with magnetic fields in unprecedented ways and have motivated materials scientists to find new methods for generating twisted electrons and measuring their OAM content. Here, we provide an overview of such techniques along with an introduction to the exciting dynamics of twisted electrons.

ARTICLE HISTORY
Received 30 November 2017
Accepted 9 December 2017

KEYWORDS
Electrons; orbital angular momentum; quantum physics; nanophysics; matter waves and particle beams

1. Introduction

The analysis of physical entities through their influence on the trajectories of particles has long been of vital importance in various areas of classical physics. The ability to do so arises from the deterministic nature of the equations of motion (via Newtonian or Lagrangian mechanics), which allows the complete reconstruction of the underlying physics of a system by analyzing the trajectories of particles in motion. This scheme is used in various applications, such as mass spectrometers and alike. However, such an analysis is quickly rendered obsolete in scenarios where effects related to quantum mechanics become relevant. More specifically, these effects are a result of complementarity, which states that quantum objects are defined by properties that cannot be simultaneously observed with full certainty, such as position and momentum. Hence, the trajectories of particles are not deterministic anymore, and such an analysis becomes cumbersome.

A quantum object is additionally described by a wave nature associated with its wave function, $\Psi(\mathbf{r})$, which satisfies the Schrödinger equation. The limitations of the aforementioned classical analysis are associated with the probabilistic nature of the measurement process. Namely, one cannot in a single measurement determine the wave function $\Psi(\mathbf{r})$; one cannot determine its Fourier transform $\Psi(\mathbf{p})$ describing the distribution of the momentum variable conjugate to position. The probability of finding the particle at position $\mathbf{r}$ within a volume $d^3\mathbf{r}$ is given by $|\Psi(\mathbf{r})|^2\, d^3\mathbf{r}$. Likewise, the probability that the particle has the momentum $\mathbf{p}$ within a momentum space volume $d^3\mathbf{p}$ is given by $\left|\Psi(\mathbf{p})\right|^2 d^3\mathbf{p}$ [1]. Consequently, the complete physical description of the object is contained within its wavefunction, and can be extracted from it with the proper operators. In some specific cases, a wavefunction ψ can satisfy the equation $\hat{A}\,\psi_a = a\,\psi_a$ for a given operator $\hat{A}$. Here, ψ_a and a are said to be an eigenfunction and an eigenvalue of the operator $\hat{A}$, respectively; i.e. the object defined by ψ_a is associated with an $\hat{A}$ value of a.

Besides providing insight on the physical traits of quantum systems, such operators are also used to analyze the evolution of a system's wavefunction. Such operators most notably include the Hamiltonian, the linear momentum, and the angular momentum operators, which respectively allow to predict the time-evolution of the wavefunction as well as translations and rotations in space. The Hamiltonian is perhaps the most familiar of the three as its eigenvalues happen to be those of the Schrödinger equation and provide the energy values defining the system. The linear momentum is also fairly

CONTACT Ebrahim Karimi ekarimi@uottawa.ca

known due to its frequent appearance in the formulation of wavepackets. As for angular momentum, due to its association with rotational symmetry, it is frequently encountered when constructing the eigenfunctions of rotationally-symmetric systems such as those involving atomic potentials. However, the properties of this operator do not necessarily restrict the usefulness of angular momentum to rotationally symmetric scenarios. In fact, angular momentum can also be of relevance in cases involving wavepackets linked to the momentum operator. As later demonstrated in the following section, the free-particle Schrödinger equation allows for Gaussian wavepacket solutions defined by a certain momentum spread that is centered around a certain momentum value. However, when the wavefunction consists of momentum components oriented along the azimuth of the wavepacket's propagation, it also carries orbital angular momentum (OAM). Therefore, in addition to linear motion attributed to its *longitudinal* momentum, a certain form of azimuthal motion will be bestowed upon the wavepacket as well. When this wavepacket is associated with a charged particle, this form of azimuthal motion gets directly translated to magnetic properties. Because these properties are directly related to those of the wavefunction, any modification to these magnetic properties caused by external perturbations will be reflected in corresponding variations in this entity's wavefunction. In principle, these variations can be extracted by means of methods used to perform measurements on waves, which could involve interference or holography for instance, in order to provide information on what perturbed the wavepacket. Hence, charged wavepackets that carry OAM have the ability to probe multiple sources of perturbation.

In recent years, there has been significant progress in using electron wavepackets for such purposes [2–5]. Here, we provide an overview of the underlying attributes pertaining to the quantum formulation of free electrons carrying OAM and how they are modified by the presence of external electromagnetic fields. We also discuss recent advances regarding the generation and the detection of such wavefunctions along with applications.

2. Formulation of free electrons

We proceed with the construct of free electron wavefunctions $\Psi(\mathbf{r};t)$ carrying OAM. These wavefunctions must first and foremost satisfy the free-particle Schrödinger equation given by

$$-\frac{\hbar^2}{2m_e}\nabla^2\Psi(\mathbf{r};t) = i\hbar\frac{\partial}{\partial t}\Psi(\mathbf{r};t), \tag{1}$$

where ∇^2 is the Laplacian, $\hbar = 1.05\times10^{-34}$ J·s and $m_e = 9.11\times10^{-31}$ kg are the reduced Planck constant and the rest mass of the electron, respectively. Let us now assume that our electrons possess a well-defined central energy $\mathcal{E}_0$ and hence a momentum $p_0 = \left(2m_e\mathcal{E}_0\right)^{1/2}$. Based on this consideration, the formulation of the wavefunction is reduced to $\Psi(\mathbf{r};t) = \psi(\mathbf{r})\exp\left(-i\mathcal{E}_0t/\hbar\right)$, thus allowing us to transition towards the time-independent Schrödinger equation. In this case, the latter reduces to the Helmholtz equation $\left(\nabla^2+k^2\right)\psi(\mathbf{r}) = 0$, where $k^2 = 2m_e\mathcal{E}_0/\hbar^2$. Alternatively, this result can also be obtained within a good approximation from the Dirac equation, a relativistic version of the Schrödinger equation, and the corrected energy-momentum dispersion relation.

$$k^2 = \frac{2m_e\mathcal{E}_0}{\hbar^2}\left(1+\frac{\mathcal{E}_0}{2m_ec^2}\right), \tag{2}$$

where c is the speed of light in vacuum.

The explicit solutions to this equation will be discussed in the following sections. Before doing so, we will provide a brief description of the features that should describe them and how they manifest themselves into exotic properties. We must first pick a convenient coordinate system that accurately reflects the symmetry of electrons carrying OAM. In particular, we are looking to formulate a wavepacket propagating along a longitudinal direction defined by transverse azimuthal momentum components. This consideration suggests that the solutions should be expressed in terms of cylindrical coordinates (ρ,φ,z). The next step in formulating the wavefunction of a twisted electron is to ensure that they carry OAM, i.e. that they are eigenstates of an OAM operator. The fact that these wavepackets have a well defined longitudinal propagation, i.e. the z axis, implies that the z component of the OAM operator $\hat{L}$ should represent the OAM carried by the electron. In cylindrical coordinates, this operator is given by $\hat{L}_z = -i\hbar\left(\mathbf{r}\times\nabla\right)_z = -i\hbar\,\partial_\varphi$. It thus follows that the eigenstates of this operator must clearly have the form $\psi(\mathbf{r}) = f(\rho,z)\exp(i\ell\varphi)$, where f is a function of the radial and longitudinal coordinates and ℓ is an integer that ensures that $\psi(\mathbf{r})$ is single-valued for all values of φ. The OAM eigenvalues of these states are $\hbar\ell$, which implies that electrons defined by these wavefunctions carry quantized OAM values of $\hbar\ell$. The final step is to connect these OAM eigenstates to those of the Schrödinger equation. Namely, given that the free particle Hamiltonian describing electrons is azimuthally symmetric, it can be expected to commute with $\hat{L}_z$, thus implying that the two operators can share the same eigenstates. Therefore, not only do solutions of the form $\psi(\mathbf{r}) = f(\rho,z)\exp(i\ell\varphi)$ carry OAM, but they can also satisfy the Schrödinger

equation and thus provide a general form describing the wavefunctions of twisted electrons.

A quick glance at the dynamics of such wavefunctions can also be taken by examining its probability density current $\mathbf{j} = -i\hbar(\psi^*\nabla\psi - \psi\nabla\psi^*)/2m_e$. As mentioned earlier, OAM relates to the relative azimuthal motion of the wavepacket and should therefore be related to the φ component of the probability current. A quick calculation reveals that $\mathbf{j}_\varphi = \hbar\ell\left|f(\rho,z)\right|^2/m_e\rho$, thus verifying that there is indeed a form of quantized azimuthal motion in a twisted electron's wavefunction that is directly proportional to its OAM eigenvalue. Moreover, because electrons are charged entities, this probability current locally manifests itself as a loop of electrical current which in turn causes the electron itself to acquire magnetic attributes. One of the most useful of these properties consists of a magnetic dipole moment, whose direction and amplitude depends on the sign and the absolute value of ℓ, respectively. As discussed in later sections, it is this trait that allows twisted electrons to be generated, detected, and applied in ways that cannot be extended to other types of OAM-carrying waves.

2.1. Bessel electron beams

The complete solution describing twisted electrons can be obtained by solving the Helmholtz equation in cylindrical coordinates by using separation of variables. Its solutions take the form $\psi^{\text{Bessel}}_{\ell,k_\rho}(\rho,\varphi,z) \propto J_{|\ell|}(k_\rho\rho)\ \exp(ik_z z)\ \exp(i\ell\varphi)$, where ℓ is an integer, $J_{|\ell|}(.)$ is the ℓ^{th} order Bessel function of the first kind, and k_ρ and k_z are respectively the radial and z-oriented components of the wavefunction's wavevector such that ${k_\rho}^2 + {k_z}^2 = k^2$, e.g. see [6]. These wavefunctions are often referred to as Bessel electron beams. As expected from previous discussions, these solutions include an $\exp(i\ell\varphi)$ term in their formulation thus implying that they carry OAM. Bessel beams also have a distinct doughnut-shaped transverse profile caused by the presence of the Bessel function in their formulation. These transverse profiles can be found in Figure 1.

Though it appears at first glance that we have found a suitable wavefunction to describe OAM-carrying electrons, a closer inspection of its probability density function, $\mathcal{P}_{\text{Bessel}} = \left|\Psi^{\text{Bessel}}_{\ell,k_\rho}(\mathbf{r};t)\right|^2 = \left|\psi^{\text{Bessel}}_{\ell,k_\rho}(\mathbf{r})\right|^2$, reveals that it suffers from certain *unphysical* aspects. This probability density is explicitly given by $\mathcal{P}_{\text{Bessel}} = \left|J_{|\ell|}(k_\rho\rho)\right|^2$ and has no dependence whatsoever neither on time, φ, nor z. This directly implies that the probability of finding the *travelling* electron at position $\mathbf{r}$ does not vary with time nor position on the axis along which its wavefunction propagates. There are even more traits that add to this solution's unphysical behaviour. Unlike along the z direction, $\mathcal{P}_{\text{Bessel}}$ varies with the radial coordinate thus implying that the probability of finding the electron varies with its transverse position and holds cylindrical symmetry. The latter vanishes at certain radii $\rho_n = x_{\ell,n}/k_\rho$, where $x_{\ell,n}$ is the n^{th} zero of $J_{|\ell|}(.)$, i.e. $J_{|\ell|}(x_{\ell,n}) = 0$. This spatial probability distribution thereby forms an infinite set of concentric rings in which the probability of finding an electron is equally likely, i.e.

$$\int_{\rho_n}^{\rho_{n+1}} \left|J_{|\ell|}(k_\rho\,\rho)\right|^2\,\rho\mathrm{d}\rho = \text{constant}. \tag{3}$$

Therefore, the integral of $\left|\psi^{\text{Bessel}}_{\ell,k_\rho}\right|^2$ over a transverse plane is infinite, thus implying that the electron's wavefunction is not square-integrable and thereby cannot physically represent a probability amplitude. Though unphysical, it is worth noting that there are approximated versions of these Bessel beams exhibiting similar yet physical traits and that can be readily produced in practice using techniques that will be later discussed [7,8].

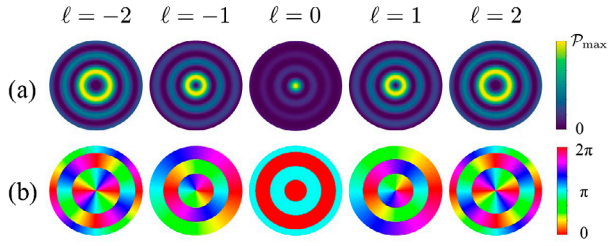

Figure 1. Transverse profile of Bessel electron waves. (a) Transverse probability density function of Bessel beams $\psi^{\text{Bessel}}_{\ell,k_\rho}$ and (b) their corresponding transverse phase profiles plotted in hue colours.

2.2. Paraxial electron wavepackets and Laguerre-Gauss beams

The unphysical nature of Bessel electron beams stems from the fact that the Helmholtz equation admits diffraction-free plane-wave solutions that are not square-integrable. To find more physical solutions, we must therefore proceed by going back to the Helmholtz equation and modifying it in order to account for the expected physical behaviour of electron wavepackets, i.e. their diffraction. Assuming that the electron's momentum is predominantly oriented along the z axis, the time-independent wavefunction becomes $\psi(\mathbf{r}) = \phi(\mathbf{r})\ \exp(ip_0 z/\hbar)$. We then re-express the Helmholtz equation in terms of $\phi(\mathbf{r})$. In order to seek for *realistic* solutions, we will be using dimensionless coordinates that are normalized to parameters describing the beam's transverse and longitudinal features. We let $\rho = w_0\,\rho'$ where ρ' is a

dimensionless radial coordinate and w_0 is the wavefunction's 'width' indicating the relative extent of the beam's transverse profile. Interestingly, a wave's width, together with its energy or its momentum along the direction of propagation, defines its diffraction. Namely, the distance over which the wave does not significantly diffract is given by $z_R = kw_0{}^2/2$. Recall that the beam energy $\mathcal{E}_0$ determines the electron's de Broglie wavelength λ_{dB}, and consequently its k value, i.e. $k = 2\pi/\lambda_{\mathrm{dB}} = (2m_e\mathcal{E}_0/\hbar^2)^{1/2}$. This relation naturally implies that the z-coordinate must be normalized in terms of z_R, i.e. $z = z_R z'$ where z' is the longitudinal dimensionless coordinate. We note that the azimuthal coordinate does not require such a normalization as it is not defined by any units, i.e. $\varphi = \varphi'$. When these dimensionless coordinates are brought into consideration, the Helmholtz equation becomes

$$\left(\nabla_{\perp}^{\prime 2} + 4i\frac{\partial}{\partial z'} + \frac{1}{\pi^2}\left(\frac{\lambda_{\mathrm{dB}}}{w_0}\right)^2\frac{\partial^2}{\partial z'^2}\right)\phi(\rho', \varphi', z') = 0, \tag{4}$$

where $\nabla_{\perp}^{\prime 2}$ is the dimensionless transverse Laplacian. We then proceed in the same way as paraxial optics, by considering electron waves with beam widths that are greater than the de Broglie wavelength, i.e. $w_0 \gg \lambda_{\mathrm{dB}}$. This is known as the paraxial approximation and effectively removes the last term of Equation (4) thus yielding the so-called paraxial wave equation. Like the Helmholtz equation, the paraxial equation admits various sets of eigenfunctions with formulations that depend on the coordinate system in which it is solved. The OAM-carrying solutions expressed in terms of cylindrical coordinates are known as the Laguerre-Gauss (LG) modes and their formulation is provided below

$$\begin{aligned}\psi_{\ell,p}^{\mathrm{LG}}(\rho,\varphi,z) = &\left(\frac{2\,p!}{\pi\,(p+|\ell|)!}\right)^{1/2}\frac{1}{w(z)}\left(\frac{\rho\sqrt{2}}{w(z)}\right)^{|\ell|}\\ &\times\exp\left(-\frac{\rho^2}{w^2(z)}\right)L_p^{|\ell|}\left(\frac{2\rho^2}{w^2(z)}\right)\\ &\times\exp\left(i\Phi_{\ell,p}^{\mathrm{LG}}\right),\end{aligned} \tag{5}$$

where $w(z) = w_0(1 + (z/z_R)^2)^{1/2}$ is the electron beam's spot size, $L_p^{|\ell|}(.)$ is the associated Laguerre polynomial, and $\Phi_{\ell,p}^{\mathrm{LG}}$ consists of the phase of the beam and is given by

$$\begin{aligned}\Phi_{\ell,p}^{\mathrm{LG}} = &\frac{k\,\rho^2}{2R(z)} + \ell\varphi + kz\\ &-\left(2p + |\ell| + 1\right)\arctan\left(\frac{z}{z_R}\right),\end{aligned} \tag{6}$$

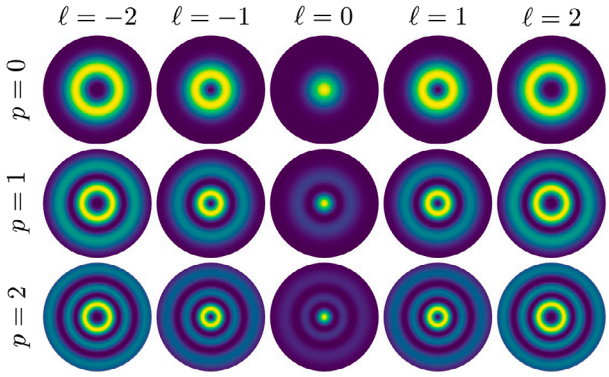

Figure 2. Transverse profile of Laguerre-Gauss electron waves. Transverse probability densities of various Laguerre-Gauss beams $\psi_{\ell,p}^{\mathrm{LG}}$. Notice the increase of the beam's extent with increasing ℓ and the addition of supplementary intensity rings with increasing p.

where $R(z) = z(1 + (z_R/z)^2)$ describes the beam's wavefront curvature upon propagation. The last term in Equation (6), i.e. $\arctan(z/z_R)$, is referred to as the Gouy phase, and anomalously changes its sign upon traversing through $z = 0$. For $\ell \neq 0$, LG modes are also characterized by doughnut shaped transverse probability distributions. Moreover, the counterpart to the continuous variable k_ρ that radially modulates the wavefunction's profile in Bessel beams is the discrete variable $p \geq 0$. Thus, unlike Bessel solutions which are only azimuthally quantized by the index ℓ, the LG solutions are also radially quantized. This distinct attribute is readily seen in these beams' transverse structures which are shown in Figure 2.

LG wavefunctions are also defined by the very physical attributes that the Bessel wavefunctions lack. In particular, we can see that these wavefunctions experience diffraction broadening given that the extent of their transverse distributions is defined by $w(z)$ while the curvature of their wavefronts is set by $R(z)$, both of which vary upon propagation. Moreover, the integral of the probability density $\mathcal{P}_{\mathrm{LG}} = |\psi_{\ell,p}^{\mathrm{LG}}|^2$ over the transverse plane is normalized to unity. An additional modulation to the longitudinal component of $\psi_{\ell,p}^{\mathrm{LG}}$ can also provide a means to make the integral of $|\psi_{\ell,p}^{\mathrm{LG}}|^2$ finite over z. This modulation typically consists of a Gaussian distribution ensuring that the resulting wavefunction is still a solution of the paraxial wave equation with the properties of LG wavefunctions [9]. This modulation enforces a quantization of the longitudinal structure of electron waves defined by *moving* Hermite-Gauss modes, i.e.

$$\phi_{\ell,p,n}(r,\varphi,z;t) = \psi_{\ell,p}^{\mathrm{LG}}(r,\varphi;t)\,u_n^{\mathrm{HG}}(z - (p_0/m_e)t) \tag{7}$$

where $u_n^{\mathrm{HG}}(.)$ are the Hermite-Gauss modes with n being a positive integer value. The 3+1 dimensional wavepacket solutions form a complete orthonormal set of modes.

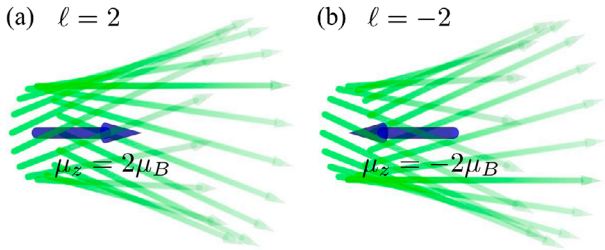

Figure 3. Magnetic dipole moment and classical trajectories of an electron beam. The trajectories are illustrated over half a diffraction length $z_R/2$ for the cases of (a) $\ell = 2$ and (b) $\ell = -2$.

That is, $\langle \phi_{\ell,p,n} | \phi_{\ell',p',n'} \rangle = \int \phi^*_{\ell,p,n} \phi_{\ell',p',n'} \, d^3\mathbf{r} = \delta_{\ell,\ell'} \delta_{p,p'} \delta_{n,n'}$, where $\delta_{i,i'}$ is the Kronecker delta function. Thus, any solution of the paraxial wave equation $\chi(r, \varphi, z; t)$ can be expressed as a superposition $\chi(r, \varphi, z; t) = \sum_{\ell,p,n} c^{\ell,p,n} \phi_{\ell,p,n}(r, \varphi, z; t)$, where $c^{\ell,p,n}$ are expansion coefficients. As expected, the Laguerre-Gauss modes have an $\exp(i\ell\varphi)$ term in their formulation. Therefore, just like Bessel electron beams, this term makes the $\phi_{\ell,p,n}$ wavepackets eigenfunctions of the $\hat{L}_z$ operator with eigenvalues $\hbar\ell$. As discussed earlier, the OAM carried by such an electron will be given by $\hbar\ell\,\mathbf{e}_z$, thus causing the electron to carry a magnetic dipole moment of $\boldsymbol{\mu} = g\mu_B \ell\,\mathbf{e}_z$. Here, $g = 1$ is the g-factor for the electron orbital motion, $\mu_B = e\hbar/2m_e$ is the Bohr magneton, and $\mathbf{e}_z$ is the unit vector in the z direction. This magnetic moment is illustrated in Figure 3 for the cases of electron wavefunctions of OAM $\ell = \pm 2$ along with the classical trajectories attributed to the latter.

Though this value was deduced from the electron's OAM and its classical gyromagnetic ratio, it can also be extracted from the formulation of the electron's wavefunction. More specifically, the motion attributed to $\Psi(\mathbf{r}; t)$ causes it to acquire a probability density current given by $\mathbf{j} = m^{-1}[\mathcal{P} p_0\,\mathbf{e}_z + \hbar\,\mathrm{Im}(\phi^* \boldsymbol{\nabla}\phi)] \simeq m^{-1}\mathcal{P}(p_0\,\mathbf{e}_z + \hbar\ell\mathbf{e}_\varphi/\rho)$, where $\mathcal{P} = |\phi|^2$ is the electron's transverse probability density distribution [9]. Because the distribution of the electron's charge and its mass are both proportional to the probability density function of the wavefunction, it follows that this probability current density can be translated into an electrical current density of $e\mathbf{j}$, where e is the electron's charge. Therefore, we can see that the electron's magnetic dipole moment comes from the electron's azimuthal current density $J_\varphi \simeq e(\hbar\ell/m_e\,\rho)\mathcal{P}$.

3. Generation

Early realizations of free OAM-carrying electrons at sub eV energies exploited the fact that bound electrons in atoms can be attributed to OAM ($\hat{L}_z$) eigenstates in conjunction with ionization processes that remove such electrons from atoms. Namely, upon ionization, the emitted electron will carry OAM defined by its former atomic eigenstate [10]. Moreover, if for instance an atom that is in a superposition of two electronic angular momentum states is ionized, the emitted electron will likewise be in a superposition of two angular momentum states leading to quantum beats, which have been observed in both, field ionization [11] and photoionization [12].

Our previous discussions concerning the formulation of electron wavefunctions have revealed that the net OAM carried by an electron explicitly relies on the presence of an $\exp(i\ell\varphi)$ term. In practice, imprinting such an azimuthally varying transverse phase onto an incident Gaussian electron beam results in the generation of an OAM-carrying electron beam. Shaping electron beams into OAM-carrying beams can be achieved through a variety of methods, four of which are outlined below. Unlike earlier methods relying on ionization, the ones presented in this section are designed to generate coherent electron waves. Furthermore, they are also more easily implemented in electron microscopes, in which procedures to characterize materials using twisted electrons are usually implemented.

3.1. Spiral phase plates

The azimuthal phase dependence of OAM carrying wavefunctions causes their wavefronts, i.e. regions of constant phase, to be helically shaped. In essence, *spiral phase plates* (SPPs) are devices that directly impose such a twisted wavefront. They are made of a material possessing a mean inner potential $V_{\mathrm{inner}}(\mathbf{r})$ that can be effectively seen as a potential barrier by the electrons. As a result, when the electrons travel through such a material, they will lose kinetic energy and thus momentum. Therefore, their de Broglie wavelength increases within the material, as prescribed by the relation $\lambda_{\mathrm{dB}} = h/p$. With this increase, one is therefore capable of arbitrarily shaping an electron beam's wavefront using a slab of this material with a correspondingly varying thickness. Namely, the introduced phase shift due to a material with a thickness $t(\mathbf{r})$ is $\chi(\mathbf{r}) = C_E V_{\mathrm{inner}}(\mathbf{r})\, t(\mathbf{r})$, where C_E is a constant. SPPs consist of such slabs that are specifically designed to have a spiraling thickness profile, i.e. $t(\mathbf{r}) := t(\varphi) = a + b\,\varphi$, where a and b are two arbitrary real parameters. When $\oint d\chi(\mathbf{r})$ is set to $\ell\lambda_{\mathrm{dB}}$, i.e. integer multiples of wavelength, then the SPP imprints a spiraling wavefront consisting of ℓ intertwined helices onto the traversing electron beam's wavefunction, and thus causes it to acquire ℓ units of OAM as illustrated in Figure 4(a). It is worth mentioning that the generated beam is neither Bessel nor LG, because it is generated via a direct imprinting of a phase singularity $\exp(i\ell\varphi)$ onto a Gaussian probability distribution, i.e. $\exp(i\ell\varphi)\,\exp(-\rho^2/w_0^2)$. Such

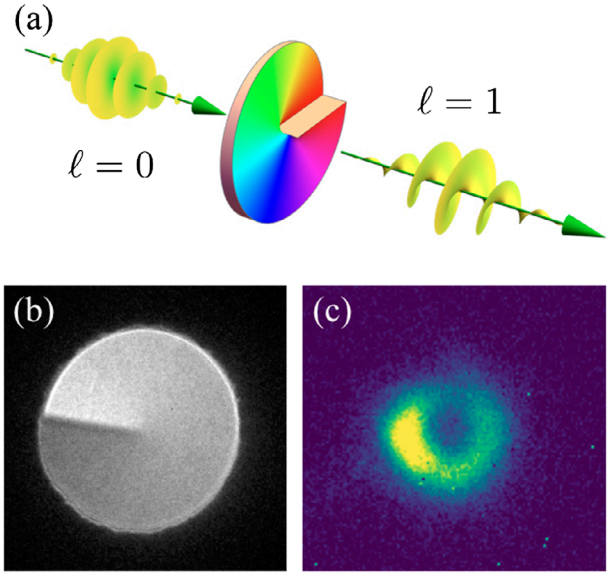

Figure 4. Shaping an electron wave to imbue it with orbital angular momentum (OAM). (a) The process of imparting one unit of OAM onto an electron through the use of a spiral phase plate. The thickness of the phase plate is emphasized by a hue colour scheme where areas coloured in red represent a thickness corresponding to an integer multiple of the electron's wavelength. (b) TEM bright field image of a spiral phase plate designed to generate electrons carrying ℓ=1 units of OAM. (c) Probability density of the electron beam generated with the spiral phase plate shown in (b).

modes are referred to as a sub-class of Hypergeometric-Gauss modes, and unlike LG and Bessel beams, they are not shape-invariant upon free-space propagation. The first electron SPP was reported in 2010 by Uchida and Tonomura who used spontaneously stacked graphite thin films for a 300 keV electron beam and have reported the first generation of electron vortex beams [13]. Since then, significant improvements have been made in nano-fabricating such devices [14]. A TEM image of an SPP fabricated using ion beam lithography along with the electron beam generated from the device is shown in Figure 4(b) and (c), respectively.

3.2. Holography

As opposed to SPPs, which directly shape the wavefronts of electron beams, the generation of OAM-carrying electrons through the use of holography relies on the distinct interference pattern of an OAM carrying wavefunction, $\psi_\ell(\mathbf{r}) \propto \exp(i\ell\varphi)$, with reference electron waves $\psi_{\text{ref}}(\mathbf{r})$. More specifically, holography consists of generating an image $\psi_{\text{image}}(\mathbf{r})$ from the pattern resulting from its interference with a slightly misaligned plane wave $\psi_{\text{ref}}(\mathbf{r}) \propto \exp(ik_y y)$, i.e. $I(\mathbf{r}) = |\psi_{\text{image}}(\mathbf{r}) + \psi_{\text{ref}}(\mathbf{r})|^2$. Here, k_y is a transverse component of the wave vector and we will omit the propagating phase term $\exp(ik_z z)$ in the formulation of the reference and image wavefunctions. Thus,

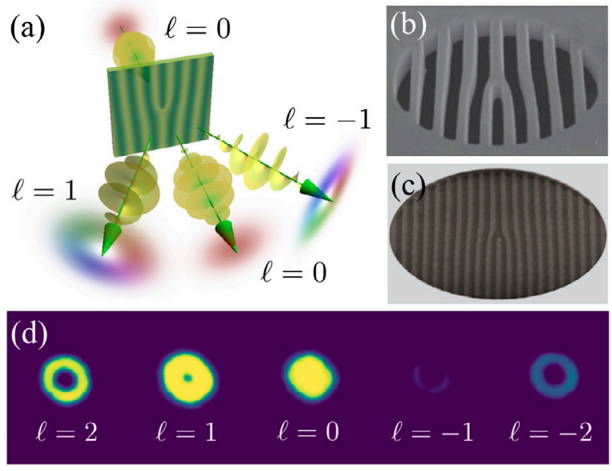

Figure 5. Shaping twisted electrons with amplitude and phase holograms. (a) Depiction of the holographic generation of OAM-carrying electrons, (b) SEM image of an electron amplitude mask reported by Verbeeck et al. [15], (c) SEM image of an electron phase mask reported by Grillo et al. [16]. (d) Experimental diffraction intensity pattern of a pitchfork hologram in which the OAM carried by each diffraction order is noted.

having such a pattern, $I(\mathbf{r})$, for the case where the image corresponds to the OAM-carrying beam, i.e. $\psi_{\text{image}}(\mathbf{r}) = \psi_\ell(\mathbf{r})$, would provide one with the means of generating it. Assuming that the reference and OAM-carrying beams are equally weighted, this interference pattern is given specifically by $I(\mathbf{r}) \propto (1 + \cos(\ell\varphi - k_y y))$ and has the appearance of a pitchfork. Using holography, one can make a hologram with this pattern in order to generate the corresponding OAM-carrying beam by reversing the interference process described above. Namely this reverse process consists of illuminating the pitchfork hologram with an electron plane wave and thereby producing an OAM-carrying beam that is misaligned with respect to the plane wave. Such holograms can be used in two different forms; (i) as amplitude masks [15], and (ii) as phase masks [16–18]. The amplitude mask is a partially absorbing device that directly modulates an incoming electron's wavefunction ψ_0 to $\psi_0(1 + \cos(\ell\varphi - k_y y))$, or equivalently, $\psi_0\big(2 + \exp(i(\ell\varphi - k_y y)) + \exp(-i(\ell\varphi - k_y y))\big)$. The latter formulation of the transmitted wavefunction directly implies that it consists of three distinctly propagating waves: one that is not deflected, another deflected in the $-k_y$ direction, and another deflected in the $+k_y$ direction where the latter two carry OAM values of $+\hbar\ell$ and $-\hbar\ell$ respectively. As opposed to amplitude masks, phase masks, sometimes referred to as kinoforms, rather modify an electron wavefunction by a phase factor $\exp(i\,I(\mathbf{r}))$. Though these devices are often still characterized by some forms of absorption, this absorption is not nearly as important as the imparted phase modulation. The low absorption causes the efficiencies of phase holograms to be much higher than those of

amplitude masks. Other than the considered sinusoidal holograms, it is worth noting that these amplitude and phase masks can also adopt blazed and binary configurations. An illustration of the holographic generation of twisted electrons is shown in Figure 5(a). SEM images of holograms reported by Verbeeck et al. [15] and Grillo et al. [16] can be found in Figure 5(b) and (c), respectively. We also provide an experimental diffraction intensity pattern of such a hologram in Figure 5(d).

3.3. Magnetic monopole

Unlike the SPPs and holographic techniques that directly use the wave nature of electrons for OAM impartment, the present method additionally employs the electron's charge. Namely, when traveling along a certain path C while being affected by a vector potential $\mathbf{A}$, an electron will acquire a phase given by $\chi = (e/\hbar)\int_C \mathbf{A}\cdot d\mathbf{r}$. We may choose to express this phase as a relative phase with respect to that acquired by an electron while traveling along a given reference path [19]. Therefore, upon this supplementary consideration, the phase acquired by the electron along path C can be expressed as a closed loop integral which, in addition to C, considers this reference path, hence $\chi = (e/\hbar)\oint_C \mathbf{A}\cdot d\mathbf{r}$ [20]. Using Stokes' theorem, this integral can be rearranged as a surface integral over $\nabla\times\mathbf{A}$, which is defined by the applied corresponding magnetic field $\mathbf{B}$. Such a rearrangement causes the form of the acquired phase to change to $\chi = (e/\hbar)\,\Phi_B$, where $\Phi_B = \int_S \mathbf{B}\cdot d\mathbf{s}$ is the magnetic flux going through the closed loop C. Therefore, the global phase gained by the electron is proportional to the magnetic flux passing through the surface embedded by C. Let us now consider the case where $\mathbf{B}$ corresponds to the field attributed to a magnetic monopole, i.e. $\mathbf{B} = (\mu_0 q_m)/(4\pi r^3)\,\mathbf{r}$, where μ_0 is the permeability of free-space, $r = |\mathbf{r}|$ is the radial coordinate, and q_m is the strength or the 'magnetic charge' of the monopole. As depicted in Figure 6(a), the flux going through the surface delimited by the electron's trajectory and a reference trajectory positioned at $\varphi = 0$ clearly depends on the azimuthal separation $\Delta\varphi = \varphi$ between both paths. Indeed, a calculation of this flux reveals that the phase acquired by the electron beam becomes $\chi = (e\,\mu_0 q_m)/(h)\,\varphi$. We can therefore see that a magnetic monopole can add an azimuthally dependent phase to the electron. When $(e\,\mu_0\,q_m)/(h)$ is an integer, this phase can directly be associated with OAM as illustrated in Figure 6(b). Interestingly, on a fundamental level, the postulated existence of natural magnetic monopoles would enforce such a condition onto the monopole's magnetic charge q_m, i.e. the magnetic charge is intrinsically quantized. Unfortunately, the existence of these entities has so far not been

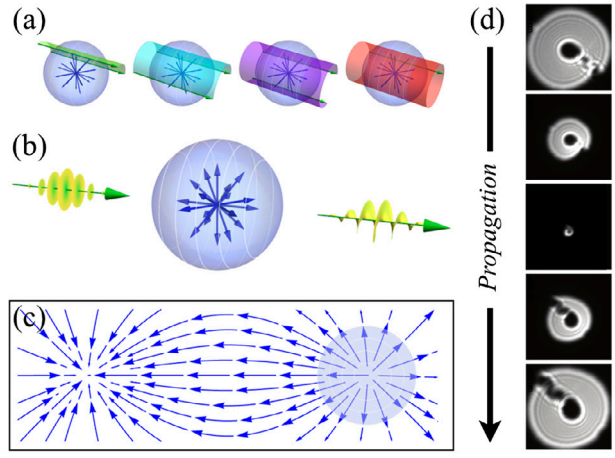

Figure 6. Electron propagation through a magnetic monopole. (a) Images of the surfaces used to calculate the phase gained by an electron upon propagating through a monopole's magnetic field. These surfaces are associated with electrons positioned at azimuthal coordinates of (left-to-right) $\varphi = \pi/2, \pi, 3\pi/2$, and 2π. (b) Illustration of an electron gaining one unit of OAM ($(e\,\mu_0 q_m)/h = 1$) upon propagating through a magnetic monopole. (c) Field lines of a magnetic dipole. The highlighted area depicts the region where this field closely resembles that of a magnetic monopole. (d) Experimental propagation of a focused OAM-carrying electron beam generated by a magnetic needle reported by Béché et al. [21].

shown, hence we cannot directly use them to impart OAM onto electrons. However, the absence of natural magnetic monopoles does not necessarily prohibit the use of entities that can imitate their magnetic structure for such purposes. For instance, as shown in Figure 6(c), one could employ one end of a magnetic dipole where the field is very close to being perfectly radial. In fact, it has been demonstrated that magnetic needles can be used in this fashion to generate OAM-carrying electrons. In essence, magnetic needles consist of very thin magnetic dipole structures whose strength can be tuned by the application of an electrical current [21]. With this tuning procedure, the 'monopole' strength q_m of both ends of the needle can be modified to satisfy the condition $\ell = (e\,\mu_0\,q_m)/h$, where ℓ is an integer, thus allowing the impartment of $\hbar\ell$ units of OAM onto incoming electrons. Nonetheless, the blocking caused by the needle will introduce a small spread in the electron's OAM spectrum. These effects can effectively be noticed in the experimental propagation of a beam generated by such means as originally reported by Béché et al. [21]. These results are shown in Figure 6(d).

3.4. q-filters

The manner in which the previous methods add azimuthal phase variations to electrons either rely on interacting with its wavefronts or with its charge. Here, we present a way to add OAM onto electrons by using another of their distinguishing traits, namely their spin, in

conjunction with an externally applied magnetic field by means of a device known as a q-filter. Much like its OAM, an electron's spin consists of a property describing a component of its total angular momentum. However, unlike OAM, spin is not related whatsoever to the electron wavefunction's spatial profile, but is rather attributed to one of its more intrinsic states. More specifically, it is attributed to the angular momentum generated by a specific component of the circulating flow of energy in the electron's wavefunction [22]. As in the case of OAM, spin consists of a quantized quantity, yet, for electrons, it is bounded to values of $s = \pm 1/2$ in units of $\hbar$. The fundamental differences between spin and OAM allows for an electron's wavefunction to be simultaneously defined by both of these properties, though it is worth noting that both forms of angular momenta couple to each other in relativistic regimes [23]. In particular, as formerly employed, the OAM component of an electron is often formulated in terms of an $\exp(i\ell\varphi)$ term in its wavefunction while its spin component is represented by $|\uparrow\rangle$ or $|\downarrow\rangle$, which respectively denote spins of $\pm 1/2$. Moreover, as in the case of OAM, an electron's spin contributes to its magnetic dipole moment by an amount $\boldsymbol{\mu} = g_s \mu_B \mathbf{s}$, where $g_s \approx 2$, thus allowing spin to effectively interact with magnetic fields. In particular, when an electron's spin precesses about an applied magnetic field, it will gain a phase. The phase acquired due to this interaction corresponds to a geometric (Berry) phase which generally describes the phase acquired by physical entities upon being subjected to cyclic adiabatic processes. In this case, this adiabatic process corresponds to the periodic precession of the electron's spin about the applied magnetic field. This precession can be attributed to a specific trajectory in the electron's spin space [20] conveniently depicted by a Bloch sphere where the north pole is associated with the $|\uparrow\rangle$ state and the south pole associated with the $|\downarrow\rangle$ state. The phase acquired by the electron will thereby depend on the trajectory that its spin vector follows on the Bloch sphere with respect to a reference trajectory. In essence, this acquired phase is proportional to the solid angle enclosed by the trajectories on the Bloch sphere.

The idea behind the q-filter, as depicted in Figure 7(a), is to enable such a precession in a systematic way that will make the electron acquire an azimuthally dependent phase, and thus OAM. To achieve such control, we make electrons defined by a central momentum p_0 go through a finite region of length L where there is a well-defined (space-varying) magnetic field. In practice, this region is usually configured as a tube of length L in which several magnets are inserted to generate a particular field. In addition to the magnetic field, an electric field is also applied inside the tube to neutralize the Lorentz force

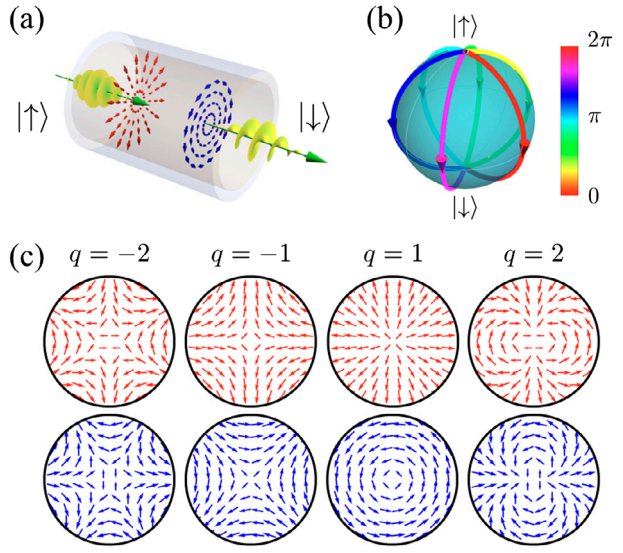

Figure 7. Electron propagation through structured magnetic fields. (a) The configuration of a $q = 1$-filter in which structured magnetic (blue) and electric (red) fields are used over a finite region to generate OAM-carrying electrons using an external form of spin-to-orbit coupling. (b) Trajectories taken by the spin-up electron state on the Bloch sphere upon precessing in a magnetic field oriented along $\varphi = \alpha$. These trajectories are coloured according to the orientation of the corresponding magnetic field. (c) Examples of structured electric (red) and magnetic (blue) fields that can be used in a q-filter configuration. Note how the fields attributed to negative q values correspond to feasible hexapole and quadrupole configurations.

applied on the electron, i.e. $e(\mathbf{E} + \mathbf{p}/m_e \times \mathbf{B}) = 0$, in order to prevent deflections in the electron's trajectory. For simplicity we first consider the case where the applied magnetic field is uniform and oriented along an angle α with respect to the x axis. Moreover, we consider the general case where electrons with no OAM are traveling along the z axis. These electrons also consist of a superposition of its possible spin states, $|\psi\rangle_{\text{in}} = a_1 |\uparrow\rangle + a_2 |\downarrow\rangle$, where a_1 and a_2 are normalized amplitude coefficients, i.e. $|a_1|^2 + |a_2|^2 = 1$. To find the wavefunction at the output of the tube, we must solve the Schödinger-Pauli equation which describes the nonrelativistic behaviour of an electron inside electromagnetic fields [24]. The electron wavefunction after interacting with balanced magnetic and electric fields is given by

$$\begin{aligned} |\psi\rangle_{\text{out}} = a_1 \left[\cos(\delta/2)\,|\uparrow\rangle + i \sin(\delta/2)\, e^{i\alpha}\,|\downarrow\rangle\right] \\ + a_2 \left[\cos(\delta/2)\,|\downarrow\rangle \right. \\ \left. + i \sin(\delta/2)\, e^{-i\alpha}\,|\uparrow\rangle\right], \end{aligned} \tag{8}$$

where $\delta = 4\pi L/\Lambda_1$, $\Lambda_1 = 4\pi R_c/g_s$, and $R_c = p_0/(|e|\,B)$ is the cyclotron radius. We can quickly deduce from this expression that the electron experiences a precession process defined by a spatial period $\Lambda_1/2$ and by an angle δ. As formerly mentioned, this causes a part

of the electron wavefunction to acquire a phase of $\pm\alpha$ attributed to the trajectory of the electron's state on the Bloch sphere as shown in Figure 7(b). However, we can see that the addition of this phase is also accompanied by a flip in the electron's spin. Such a conversion can be made complete in the case where $\delta = \pi$, which can practically be achieved by carefully tuning the physical parameters defining our system. The latter include the tube's length L, the electrons' momentum p_0, and the magnitude of the applied magnetic field B. When the magnetic field inside the tube is structured to have an azimuthally varying orientation of $\alpha(\mathbf{r}) = q\,\varphi + \beta$, where q is an integer and β is a constant, we can see that electrons will obtain a space-dependent phase of $\pm q\,\varphi$, which directly corresponds to the acquirement of OAM. Examples of such fields along with the electric fields used to neutralize the Lorentz force acting on the electron can be found in Figure 7(c). A tube configured to generate such a field is referred to as a q-filter.

Though this technique may at first appear to offer little more than OAM impartment, the fact that it explicitly relies on a form of coupling between spin and OAM allows it to be used in the following manner. Consider a spin-unpolarized electron beam carrying OAM of $\ell = 1$, i.e. $|\psi\rangle_{\text{in}} = \exp(i\varphi)(a_1|\uparrow\rangle + a_2|\downarrow\rangle)$, which could have been generated using any of the aforementioned methods. By making such a beam pass through a $q = 1$-filter that perfectly converts the original state of the electrons, we will obtain an output wavefunction $|\psi\rangle_{\text{out}} = a_1 \exp(i2\varphi)|\downarrow\rangle + a_2|\uparrow\rangle$. Let us now recall that OAM-carrying wavefunctions ψ are defined by doughnut shaped probability densities $|\psi|^2$ with a spatial extent that scales with the OAM carried by the electrons. Based on this property, we can see that the central region of $|\psi\rangle_{\text{out}}$ is almost entirely composed of electrons of spin $|\uparrow\rangle$. Therefore, by making such electrons go through a pinhole with an area that mostly encompasses the electrons of spin $|\uparrow\rangle$, one could effectively use the q-filter as an electron spin polarizer with a conversion efficiency that can realistically reach values near 97.5% [24–26].

4. Measurement

Due to their ability to add or remove well-defined units of OAM from an incident electron beam, many of the devices introduced in the previous section can alternatively be used to measure the OAM content of electrons. Practically speaking, instead of using the devices to turn Gaussian beams into OAM-carrying beams, they are employed to remove a given amount of OAM from the electrons. By doing so, electrons that originally carry the corresponding amount of removed OAM will thereby gain a Gaussian profile while electrons that do not carry this specific amount will have their OAM altered, yet their profile will still be doughnut-shaped. One can then select the electrons with the Gaussian profile, which originally carried the amount of removed OAM, by focusing the resulting beam through a pinhole. Thereafter, by looking at the relative amount of electrons contained in this Gaussian component with respect to the total number of electrons in the original beam, the weight of electrons carrying the removed amount of OAM in the original beam can be determined. This method is referred to as phase-flattening projective measurements, since the wavefronts of individual twisted electrons are flattened through the impartment of the phase of their OAM conjugate, and then post-selected by a pinhole [27].

Though this method is quite simple, it suffers from several disadvantages. The most inconvenient of them is the need to use a specific device to analyze a distinct OAM component. Therefore, to obtain the total OAM spectrum of an electron beam, one would need an amount of devices corresponding to the amount of analyzed OAM components which can make the measurement of the electron beam's OAM long, tedious, and inefficient. The fact that some of the outer electrons of the converted Gaussian component are blocked by the pinhole further reduces the efficiency of this method. Moreover, this method is biased against measuring higher values of OAM [28].

4.1. OAM sorter

The aforementioned inconveniences in conventional OAM measurement have led to the development of alternative methods to analyze an electron beam's OAM spectrum. One of the most prominent of these methods consists of a contraption that effectively behaves as an OAM spectrometer and is commonly referred to as an OAM sorter. More specifically, it is able to separate or sort electrons based on their OAM content [29,30]. The core of the method relies on unwrapping an electron wavefunction's azimuthal phase variations into variations along a given Cartesian coordinate as depicted in Figure 8(a) for beams of OAM $\ell = 0$ and $\ell = \pm 2$. The wavefronts of these unwrapped electrons will be tilted with respect to their direction of propagation and the degree to which these wavefronts are tilted increases with the original amount of OAM carried by the electrons. Once the electrons are unwrapped, they go through a magnetic lens which will focus the electrons at various positions determined by the relative tilt of their wavefronts as shown in Figure 8(b). Because the tilt in the electron wavefunction is determined by its initial OAM value, the signal resulting from this sequence of transformations consists of a series of focused points with intensities

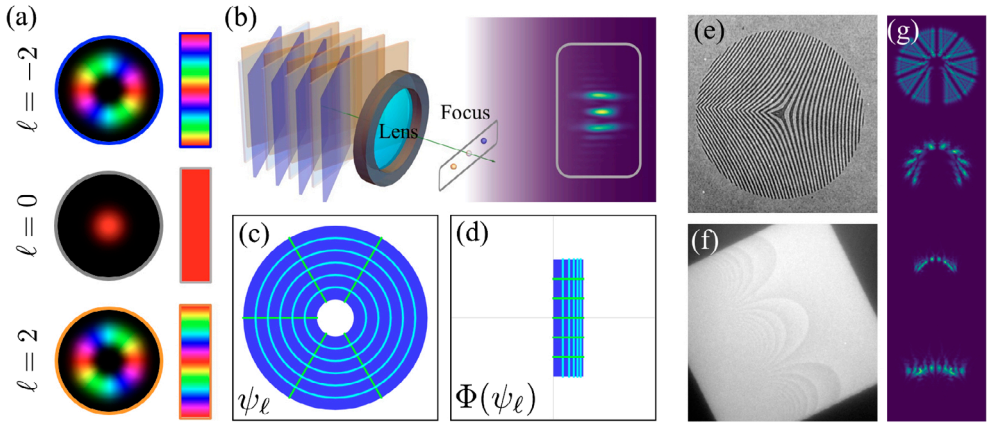

Figure 8. An electron OAM sorter. (a) Transverse phase profiles of OAM-carrying beams with $\ell = 0$ and $\ell = \pm 2$ modulated by their intensity profiles along with their unwrapped phase profiles. (b) The sorting process of these unwrapped beams where the latter go through a magnetic lens to be focused at different positions based on their original OAM values. (c) Contour lines depicting variations in the radial and azimuthal coordinates in a Cartesian system and (d) the equivalent coordinate variations in log-polar coordinates. The two systems are linked by the coordinate transformation Φ. (e) TEM bright field images of the first and (f) the second of two holograms that can be used to unwrap an OAM-carrying electron's azimuthal phase variations into linear phase gradients. (g) Simulated observed unwrapping process experienced by an electron beam consisting of a superposition of $\ell = \pm 5$ OAM components.

that directly correspond to the weight of a certain OAM component in the electron beam.

As implied earlier, the main challenge concerning the implementation of such a device consists of finding a reliable way of unwrapping the electron's azimuthal phase. In essence, this unwrapping process corresponds to a conformal mapping Φ that maps the azimuthal coordinate to a Cartesian coordinate. The mapping can take the form $\Phi(\psi) = a \ln(\psi/b)$, where ψ is a complex function. In the case where ψ corresponds to an OAM carrying wavefunction such as $\psi_\ell(\mathbf{r}) = f(r)\exp(i\ell\varphi)$, where $f(r)$ is a function of the radial coordinate, we can see that the mapping $\psi_\ell \mapsto \Phi(\psi_\ell)$ will result in the wavefunction $\Phi(\psi_\ell) = a \ln(f(r)/b) + i a\ell\varphi$ where radial variations are mapped along one Cartesian coordinate while simultaneously mapping azimuthal phase variations along the other. In practice, this mapping is realized by means of a log-polar coordinate transformation which can be performed by adding a particular phase onto an electron wavefunction. Namely, as illustrated in Figure 8(c)–(d), the azimuthal coordinate in a Cartesian system is equivalent to a standard Cartesian coordinate in a log-polar system, thus allowing for the required unwrapping. This unwrapping can be achieved using the holograms shown in Figure 8(e)–(f). Simulated data illustrating the unwrapping process enabled by the two holograms on an electron beam carrying $\ell = \pm 5$ OAM components is shown in Figure 8(g).

Such a device is of considerable interest in the materials science community due to its ability to readily provide the entire OAM content of an electron beam. Namely, material scientists often conduct works related to analyzing the effects of magnetic fields in materials on the OAM content of an electron in order to extract information concerning the material's nanoscale structure. Therefore, having such a sorter would considerably simplify such a task, as demonstrated in [29].

4.2. Nondestructive measurement

Though the above sorting process directly provides a beam's OAM spectrum, it however relies on drastically modifying the beam's wavefront. Here we provide an outline of a recent proposal involving the measurement of an electron's OAM without resorting to modifying its wavefront, and hence without modifying its OAM. To perform such a measurement, we must make use of the fact that the azimuthal probability current density of twisted electrons is given by $\mathbf{j}_\varphi \simeq \mathcal{P}(\hbar\ell/m\rho)$ which gives rise to a magnetic dipole moment $\boldsymbol{\mu} = \ell\mu_B\,\hat{\mathbf{e}}_z$. The presence of this current results in an azimuthal vector potential which can be found from $\mathbf{j}_\varphi$ by solving Poisson's equation. However, in the case where we are interested in examining the effects of this potential at radial distances that are much larger than the radial extent of the electron wavepacket, this vector potential can be simply expressed as that of a magnetic dipole. In the case of twisted electrons, it is given by $\mathbf{A}_{\text{dipole}}(\mathbf{r}) = (\mu_0/4\pi)\,\ell\mu_B\,\rho(\rho^2+z^2)^{-3/2}\,\hat{\mathbf{e}}_\varphi$ which is azimuthally symmetric and directly proportional to an electron's OAM number ℓ. Therefore, if we could measure this potential, we would be able to obtain some insight on the electron's OAM. To do so, we make the electron travel through an azimuthally symmetric hollow and conductive object such as a loop or a cylinder. Ac-

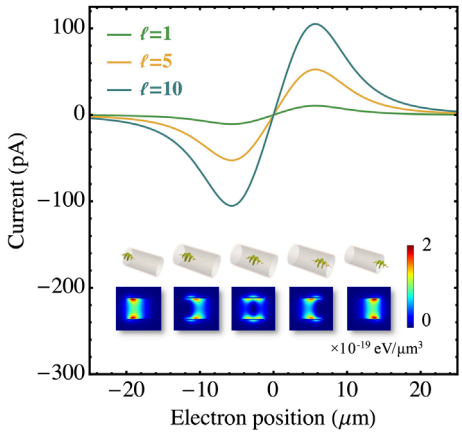

Figure 9. Nondestructive measurement of an electron's OAM. Theoretically calculated total induced currents in a conductive loop by passing electrons with OAM values of 1, 5, and 10. The density plots provided below the graph depict the magnetic energy density attributed to the magnetic field generated by the loop's currents when an electron carrying an OAM value of 100 travels through it. The corresponding position of the electron relative to the loop is depicted above each plot.

cording to Faraday's law of induction, the motion of the electron's magnetic moment will result in the generation of an electric field $\mathbf{E} = -\partial_t \mathbf{A}$ which induces a current inside the conductive loop. A quick calculation reveals that this current is also proportional to the electron's OAM number [31]. Therefore, by measuring this small yet detectable current, we should in principle be able to measure the electron's OAM. Moreover, the electron's energy can be claimed to be invariant upon propagation given that the longitudinal magnetic field generated by the loop's induced currents are only able to slow it down to a negligible fraction of its original velocity. Since the electron's canonical OAM is invariant upon propagation through a longitudinal magnetic field, then it will also not change upon propagating through such a device. The invariance of the electron's energy and OAM during this measurement process therefore causes the latter to effectively be considered as a nondestructive process (Figure 9).

5. Interaction with a longitudinal magnetic field

So far, the dynamics of twisted electrons in magnetic fields were discussed within the scope of modifying their OAM content. These discussions specifically entailed the *temporary* use of specific fields, such as that of a monopole or those with a distinct transverse topological structure, to add discrete units of OAM onto electrons via their interaction with the electron's charge or its spin. However, all of the applications regarding the generation and detection of twisted electrons were described in terms of their OAM eigenstates which also conveniently happened to be those of the potential-free Schrödinger equation. In this section, we will provide an illustration of the manner in which the eigenstates satisfying Equation (1) are modified by the presence of a uniform longitudinal magnetic field. Our discussion will closely follow the formalism employed in [32]. As in the case of the q-filter, we must proceed by finding the solutions to Equation (1) where the presence of a vector potential effectively modifies the kinetic component of the system's Hamiltonian from $-\hbar^2\nabla^2/2m_e$ to $(-i\hbar\nabla - e\mathbf{A})^2/2m_e$, where the vector potential $\mathbf{A}$ must be associated with a constant magnetic field of the form $\mathbf{B} = \nabla \times \mathbf{A} = B_0\,\hat{\mathbf{e}}_z$. Needless to say, there is more than one potential that can yield such a field, yet, due to gauge invariance, they should all be related by a gauge transformation, i.e. $\mathbf{A} \rightarrow \mathbf{A} + \nabla\chi$, where χ is a scalar. At first glance, this gauge invariance seems to imply that there could be completely different wavefunctions ψ describing our electrons in identical magnetic fields. However, it happens that these wavefunctions only differ by a phase $e\chi/\hbar$, i.e. $\psi \rightarrow \psi \exp(i\,e\chi/\hbar)$. Therefore, the dynamics of ψ, which are usually based on quantities such as $|\psi|^2$ and $\langle\psi|\,\psi\rangle$, will not be affected by these transformations. Based on such considerations, the first step in finding the eigenstates of the Schrödinger equation in the presence of a uniform longitudinal magnetic field consists of finding a convenient formulation for $\mathbf{A}$. In particular, we will consider non-zero vector potentials that yield vanishing and non-vanishing magnetic fields which respectively result in the so-called free electron *Aharonov-Bohm states* and *Landau states*. In both cases, we will let our vector potential have the form $\mathbf{A}(\mathbf{r}) = f(\rho)\,\mathbf{e}_\varphi$, thus ensuring a magnetic field defined as $\mathbf{B} = \nabla\times\mathbf{A} = \rho^{-1}\partial_\rho(\rho f(\rho))\,\mathbf{e}_z$.

Given that the vector potential has an azimuthal form, we can already intuitively see that its presence will bestow an additional form of azimuthal motion to the electrons based on the form of the kinetic momentum $\mathbf{p} - e\mathbf{A}$. In fact, the presence of the potential directly modifies the wavefunction's azimuthal probability current density to [32]

$$j_\varphi = \left(\frac{\hbar}{m_e}\mathrm{Im}(\psi^*\nabla\psi) - \frac{e}{m_e}\mathbf{A}\,|\psi|^2\right)_\varphi. \qquad (9)$$

Therefore, we can expect that the potential will either contribute or counter the electrons' intrinsic *orbital* motion.

5.1. Aharonov-Bohm states

Aharonov-Bohm states consist of *charged* wavefunctions modified by the potential $\mathbf{A}(\mathbf{r}) = (\Phi)/(2\pi\rho)\,\mathbf{e}_\varphi$, where Φ is a given magnetic flux. In its presence, the eigenfunc-

tions of the Schrödinger equation take the form

$$\psi_{\ell}^{\mathrm{AB}} \propto J_{|\ell-\alpha|}(k_\rho \rho)\exp\left(i(\ell\varphi + k_z z)\right). \tag{10}$$

where $\alpha = (e\Phi)/(2\pi\hbar)$. A quick calculation of $\mathbf{B}$ reveals that no magnetic field is actually applied on the electron [32] , given that it is essentially concentrated along the $\rho = 0$ axis. Therefore, its energy will be identical to that of a free particle. However, this cannot be said about the dynamics of the electron's wavefunction. Indeed, we can see that its original probability density function is modified to $\mathcal{P}^{\mathrm{AB}}_{|\ell-\alpha|} \propto \left|J_{|\ell-\alpha|}(k_\rho\rho)\right|^2$, thus resulting in the following probability density current

$$\mathbf{j}^{\mathrm{AB}}_{|\ell-\alpha|} = \frac{\hbar}{m_e}\left(\frac{\ell-\alpha}{\rho}\,\mathbf{e}_\varphi + k_z\,\mathbf{e}_z\right)\mathcal{P}^{\mathrm{AB}}_{|\ell-\alpha|}, \tag{11}$$

from which we can clearly observe the influence of $\mathbf{A}$ on the dynamics of the electron wavepacket. Interestingly, the wavefunction's canonical OAM $\mathbf{r}\times\mathbf{p}$ remains $\hbar\ell$. However, the expectation values of the electron's kinetic OAM $\mathbf{r}\times(\mathbf{p}-e\mathbf{A})$, which dictates the *orbital* motion of the wavepacket, are changed to $\hbar(\ell-\alpha)$. Though changes are brought to the electron's transverse dynamics, there is remarkably no variations brought to the longitudinal dynamics associated with its propagation. Most notably, the evolution of the electron's phase and its probability density function are the same as those of a free electron characterized by a quantum number $\ell \to \ell-\alpha$.

5.2. Landau states

Let us now examine the case where the electron is subjected to a potential associated with a non-zero magnetic field $\mathbf{B} = B\,\mathbf{e}_z$. To obtain such a field, we may let $\mathbf{A} = (B\,\rho)/2\,\mathbf{e}_\varphi$. The electronic eigenstates in such a field are known as Landau states [32,33] and are given by

$$\psi^{\mathrm{L}}_{\ell,p} \propto \left(\frac{\rho}{w_m}\right)^{|\ell|} L_p^{|\ell|}\left(\frac{2\rho^2}{w_m^2}\right) \times \exp\left(-\frac{\rho^2}{w_m^2}\right)\exp\left(i(\ell\varphi + k_z z)\right), \tag{12}$$

where $w_m = 2\sqrt{\hbar/(\,|eB|\,)}$ is a magnetic length parameter which holds an analogous role to the width w_0 from the paraxial Laguerre-Gauss beams that were introduced earlier [32]. Let it be noted that w_m can also be expressed in terms of the Larmor precession frequency $\Omega = (eB)/(2m_e)$ as $w_m = \sqrt{(2\hbar)/(m\,|\Omega|\,)}$.

Landau states are endowed with several key features. As previously suggested, we note that their formulation is almost identical to those of the free paraxial LG beams where the width parameter $w(z)$ is replaced by the magnetic length w_m. However, unlike the free LG beams, which are solutions to the paraxial wave equation and thereby approximate solutions of the Schrödinger equation, the Landau states $\psi^{\mathrm{L}}_{\ell,p}$ are exact solutions of the Schrödinger equation describing a charged particle exposed to a magnetic field. Moreover, unlike the width of the paraxial electrons, the magnetic length w_m is invariant upon propagation, thus causing the electron wavepacket to be diffractionless. As opposed to the Aharonov-Bohm states, the eigenenergies of the Landau states are modified by the presence of a non-zero magnetic field. These eigenenergies are given by

$$E^{\mathrm{L}}_{\ell,p} = \frac{\hbar^2 k_z^2}{2m_e} - \hbar\Omega\ell + \hbar\,|\Omega|\,(2p + |\ell| + 1). \tag{13}$$

We can see that these energies can be attributed to distinct phenomena related to the dynamics of Landau wavepackets. First and foremost, they consist of a component $(\hbar^2 k_z^2)/(2m_e)$ attributed to the longitudinal propagation of the electron. Second, they are also defined by a $-\hbar\Omega\ell$ contribution which corresponds to the Zeeman energy, $E_{\mathrm{Z}} = \mu_B \ell B$, attributed to an electron with a canonical OAM of $\hbar\ell$ in a magnetic field. Finally, these electron energies also consist of a component that is directly attributed to the discrete nature of their wavefunctions. This contribution is given by $E_{\mathrm{G}} = \hbar\,|\Omega|\,(2p + |\ell| + 1)$.

The influence of the magnetic field on the dynamics of electron wavefunctions can also be readily observed in its probability current density

$$\mathbf{j}^{\mathrm{L}}_{\ell,p} = \frac{\hbar}{m_e}\left[\frac{1}{\rho}\left(\ell + \sigma\,\frac{2\rho^2}{w_m^2}\right)\mathbf{e}_\varphi + k_z\,\mathbf{e}_z\right]\mathcal{P}^{\mathrm{L}}_{\ell,p}, \tag{14}$$

where σ denotes the sign of the magnetic field, i.e.

$$\sigma = \begin{cases} +1, & \mathbf{B} = |B|\,\mathbf{e}_z \\ -1, & \mathbf{B} = -|B|\,\mathbf{e}_z \end{cases}. \tag{15}$$

As in the case of Aharonov-Bohm states, the presence of the azimuthal vector potential effectively acts with or against the electron's canonical OAM which still has eigenvalues of $\hbar\ell$. More interestingly, we note that when the electron's OAM is countercirculating with respect to the vector potential, i.e. $\sigma\ell < 0$, then there is a critical radius $\rho_{|\ell|} = w_m\sqrt{|\ell|\,/2}$ where the wavepacket's azimuthal current density vanishes. Below this radius, the direction of the current attributed to the wavefunction's ℓ value is dominant and thus determines the current density's direction. Above $\rho_{|\ell|}$, it becomes the direction of the potential that becomes dominant. These effects cause the expectation value of the electron's kinetic OAM to have values of $\hbar(\ell + \sigma(2p + |\ell| + 1))$. Because $p > 0$, we can see

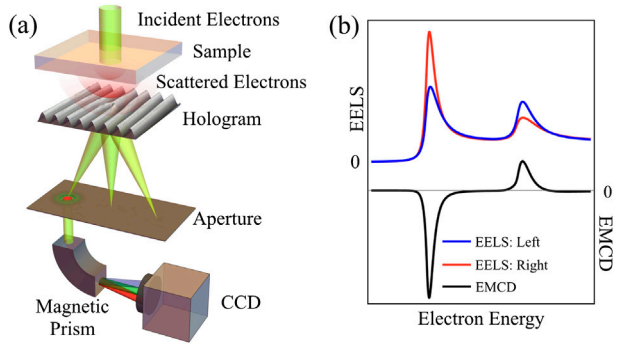

Figure 10. Probing materials with twisted electrons. (a) Illustration of an EMCD (Electron Magnetic Circular Dichroism) apparatus. A sample is exposed to an electron beam which results in the scattering of the incident electrons. A phase-flattening scheme consisting of a hologram and an aperture is then used to post-select electrons with a certain OAM value imparted by the material. A magnetic prism and a CCD camera are then used to acquire the electron energy spectrum of a particular OAM component. (b) Sketch of typical data for the electron energy loss spectra (EELS) and the corresponding EMCD spectrum in an EMCD experiment. The EELS depict the energy spectra of scattered electrons with opposite OAM values and thereby of opposite handedness (left and right). The EMCD spectrum, which corresponds to the difference between the two EELS spectra, exhibits the asymmetry between the scattered OAM components and thereby the material's magnetic properties.

that the direction of the vector potential always defines the orientation of the electron's kinetic OAM.

6. Interaction with materials

One of the main interests surrounding the practical applications of twisted electrons concerns their ability to interact with magnetic fields and thereby to be employed as nanoscale probes in magnetic materials. In practice, the use of electrons for the characterization of materials is typically implemented within a transmission electron microscope (TEM). Though traditionally employed in the context of electron imaging or diffraction experiments, TEMs have now found applications as instruments for nanoscale measurements of many material traits including magnetic or electric properties [34,35], crystalline strain [36], and phononic and plasmonic responses [37, 38]. Information pertaining to these properties can be extracted by examining how electrons are inelastically and elastically scattered by the material. These scattering processes distinguish themselves by whether a fraction of the electrons' energy is transferred to the material's internal degrees of freedom (inelastic) or whether it is constant upon propagation through the material (elastic).

The fact that experiments concerning the generation of twisted electrons can be realized within a TEM significantly facilitates their integration in the analysis of a material's attributes. The usefulness of such electrons in this context arises when their interaction with a material modifies its original OAM content thereby allowing the extraction of information concerning the potential to which it was subjected. For instance, it is well-known that the magnetic traits of ferromagnetic materials introduce a form of dichroism in an electron's inelastic scattering cross section. Namely, the degree to which twisted electrons are inelastically scattered will vary with the handedness of their helical wavefronts. This is attributed to the fact that this scattering process entails the excitation of deep atomic states with opposite symmetries and different populations. To deduce a material's magnetization from these asymmetric scattered intensities, one usually relies on its so-called electron magnetic circular dichroism (EMCD) spectra [39–42]. However, EMCD spectra have always been experimentally challenging to measure given that they originally required very sensitive inelastic wave interferometry. With the advent of electron OAM measurement techniques, the measurement of a material's dichroism has been significantly simplified to a mere analysis of an electron's OAM spectrum [15] as depicted in Figure 10. The usefulness of this technique is further extended by the fact that dichroic processes are not confined to a material's magnetic traits. In particular, based on their 3D structures, materials, or even molecules and systems of nanoparticles, can exhibit forms of dichroism in the OAM content of inelastically scattered electrons when exposed to twisted electrons. In addition to providing information on their 3D structures, the dichroism of such molecular arrangements also allows for a way of spatially resolving plasmon excitations in materials and predicting their cross section [43,44].

The characterization of a material with twisted electrons also encompasses the probing of processes that involve elastic scattering. The latter mostly involve a form of coupling between the quantum states describing twisted electrons and the material's so-called *channeling* states [45]. In principle, this coupling causes the electron to undergo a propagation that is almost undisturbed by the material. This type of propagation could prospectively allow for a characterization of the material's internal structure by examining the degree to which the state of the electron is unperturbed. However, the experimental realization of such a method has so far been prevented by the difficulties of achieving a satisfactory level of the required coupling. Even the slightest discrepancies can cause OAM-carrying electron beams to become unstable upon propagating through the material [46]. Fortunately, not all characterization methods based on the elastic scattering of OAM-carrying electrons rely on their coupling with a material's channeling states. For instance, some rely on measuring the phase acquired by OAM-carrying electrons upon propagating through a

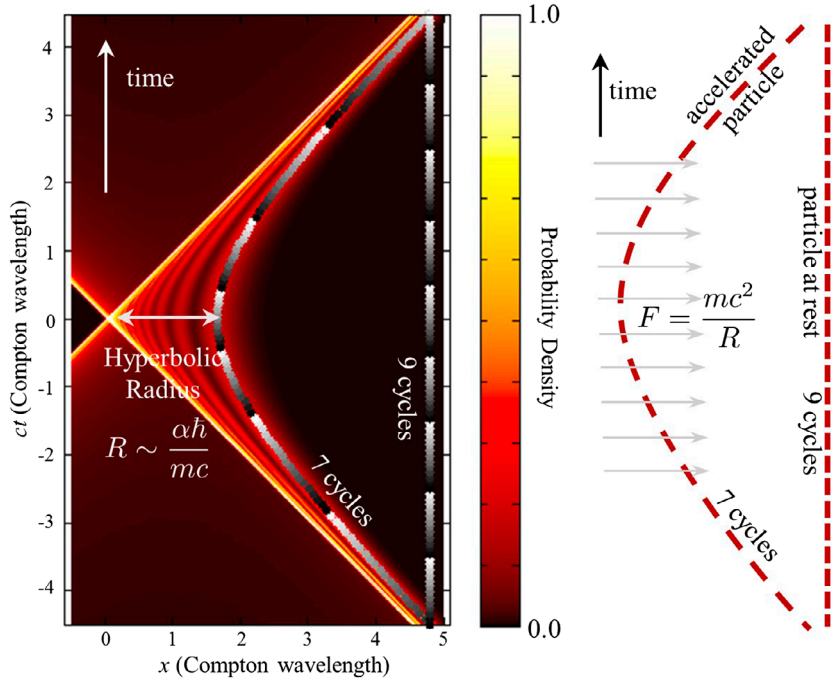

Figure 11. Inducing time dilation on a particle by shaping its wavepacket. Left: Probability density of a one-dimensional self-accelerated Dirac wavepacket on a Minkowski diagram. Right: Space-time trajectory of a relativistic particle influenced by a force $F = mc^2/R$. In both cases, the entities experience identical hyperbolic trajectories in space-time, experience the same dilation (7 time periods for the accelerated particles vs 9 time periods for a stationary particle), and acquire the same Aharonov-Bohm phase. Figure based on reference [54].

longitudinal magnetic field to essentially characterize the latter [47,48]. Another recent example consists of using OAM-carrying electrons to more easily characterize the diffraction patterns of crystals defined by more complex symmetries [49]. Beyond this, there have also been proposals concerning the application of exotic twisted electrons to impart torque to nanoparticles [50] and to produce transition radiation [51].

7. Self-accelerating twisted electrons

The influence of magnetic fields on the phase structure of electron wavefunctions undoubtedly provides a variety of ways of both generating twisted electrons and using them to characterize magnetic materials. As we have seen, other entities, such as a vector potential attributed to a vanishing magnetic field, can also influence the spatial structure of electron wavepackets. In some cases, electron wavepackets can even experience interesting phenomena in the absence of external potentials. Such effects instead arise from the initial shape and the evolution of the electron wavefunction itself.

In recent years, specially structured wavepackets designed to experience a form of 'self-acceleration' have provided new insight on the topic. Explicitly, 'self-acceleration' refers to the apparent parabolic trajectory experienced by distinct types of non-diffracting beams. In essence, the main features of the beam experience a lateral parabolic shift upon propagation, though the beam as a whole propagates along a straight trajectory. In practice, however, the finite transverse extent of wavepackets prevents them from indefinitely having this distinct parabolic structure. Instead, wavepackets will experience self-acceleration over a limited range until they eventually succumb to diffraction. Electrons defined by such self-accelerating wavepackets exist within non-relativistic regimes [52] governed by the Schrödinger equation and have been experimentally generated [53]. The recent development of self-accelerating solutions to the relativistic Dirac equation [54] has also introduced the prospect of having relativistic self-accelerating electron wavepackets defined by a variety of new properties associated with special relativity. It has in fact been shown that self-accelerating solutions of the potential-free Dirac equation [54] mimic the dynamics of a free-charge accelerating under the influence of an EM field, even though no field is present. Such wavepackets can be designed to display any effect induced by EM fields by only controlling the initial conditions of the wave pattern. Most interestingly, measurements taken along the wavepacket's trajectory cannot distinguish between a real force and this virtual force, which is self-induced by the wavepacket itself and is engineered through its initial conditions.

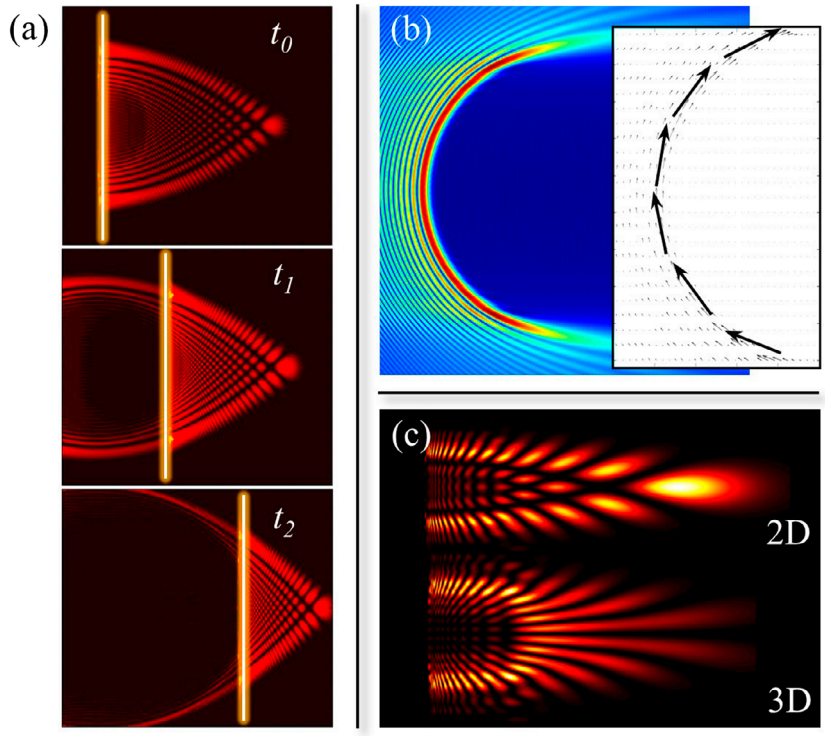

Figure 12. Families of shape-preserving wavepackets as eigenstates of symmetry operators. (a) The profile of a 2+1D accelerating electron Dirac wavepacket equation in three consequent times; the wavepacket experiences length contraction, maintaining its profile up to scaling. The glowing line marks the *ct* point in the plot. (b) The profile and the Poynting vector of an accelerating solution to Maxwell's equations, exhibiting circular self-bending of nearly 180° (figure from [55]); also equivalent to that of the massless Dirac equation of a spin 1 particle. (c) Relativistic spinless accelerating wavepackets in 2+1D (two spatial dimensions and time) and 3+1D (three spatial dimensions and time).

The measurable effects of this virtual force are real by all measurable quantities.

Another interesting property defining these self-accelerating wavepackets concerns their phase accumulation χ along the wave's trajectory. This quantity is proportional to the proper time of an equivalently accelerating particle, thus implying that the phase difference following this acceleration is equivalent to the relative time dilation between the accelerating particle and a stationary one. In practice, this relation could prospectively be used to prolong the lifetime of decaying particles by structuring their wavefunction into a self-accelerating wave [54]. The principles of these ideas are depicted in Figure 11.

In addition to these relativistic effects, the analogy between self-accelerating wavepackets and accelerating particles is of fundamental interest from an electrodynamics perspective. For instance, these similarities can lead one to question whether an electron wavefunction would emit radiation if it is shaped to self-accelerate in potential-free vacuum. While an accelerating charged particle emits Larmor (or Bremsstrahlung) radiation, it remained an open question to characterize the electromagnetic field accompanying self-accelerating particles. Their far-field behaviour is especially intriguing since it may define a regime somewhere in between the traditional non-radiating near-field and the radiating far-field while being neither – not carrying energy in the form of radiation at the far-field, yet not decaying quickly enough to be considered part of the charged particle's near-field.

Some of the exotic features of self-accelerating Dirac electrons can also be extended to other self-accelerating systems. Much like how several electron wavefunctions [7,9,13,15–18,23,53] are defined by features similar to those of optical beams [56–58], these self-accelerating features can exist in virtually any linear and nonlinear wave system in nature. For instance, such systems include plasmon waves [59–64] (some solving the full Maxwell equations [55,65]), sound waves [66,67], surface waves [68], waves on membranes, and even gravitational waves. All of these waves share a common attribute. Namely, they are part of a wider family of shape-preserving beams and wavepackets that are eigenfunctions of Lorentz operators (boosts/rotations), i.e. solutions that are invariant under the operation of any Lorentz transform. Generally, any wave system will have its shape-preserving solutions fully described by finding the eigenfunctions of its symmetry operators (see Figure 12). Consequently,

the above phenomena, such as the accumulated phases of self-accelerating particles, can be observed in various settings, e.g. optical waves in honeycomb photonic lattices [69] or in hyperbolic metamaterials [70], and matter waves in honeycomb optical lattices formed by the interference of laser beams.

In the specific case of electron wavefunctions, the self-accelerating Dirac wavepackets described above are eigenfunctions of boost operators, and in a complete analogy, Bessel beams and other vortex beams are exactly eigenfunctions of rotation operators. Hence, we can expect other families of shaped particles such as twisted (OAM-carrying) electrons, to also exhibit similar forms of 'accumulated phases' and 'extended lifetimes' when taken to their relativistic limits.

8. Conclusion

The recent surge in experimental works pertaining to the generation of twisted electrons, the framework of which was laid by previous theoretical investigations, has motivated a vast amount of studies related to the measurement of electron OAM and the interaction of charged wavepackets with electromagnetic fields. As discussed in the last section of this work, analogues to these types of interactions caused by purely relativistic effects have also been recently put forward, thus introducing a wide range of exciting phenomena. Such relativistic analyses result in wavefunctions that have completely different structures than their nonrelativistic counterparts [23,71–74] and hence, in some cases, affect the nature of their quantum dynamics. For instance, the presence of spin-to-orbit coupling in relativistic electron wavepackets directly affects the description of its coiling probability density current. The theoretical prediction of these relativistic effects thereby opens a new frontier in the field of twisted electrons. Namely, they should first motivate the inception of several experimental works aiming to detect these effects under relativistic configurations. Should these works prove successful, they will undoubtebly encourage the reformulation of several current applications relying on OAM-carrying electrons while also stimulating the emergence of several new proposals relying on the distinct behaviour of relativistic wavepackets.

Disclosure statement

No potential conflict of interest was reported by the authors.

Funding

This work was supported by Canada Research Chairs; Canada Excellence Research Chairs, Government of Canada (CERC); Natural Sciences and Engineering Research Council of Canada (NSERC); Max Planck-University of Ottawa Centre for Extreme and Quantum Photonics, and the European Union's Horizon 2020 Research and Innovation Programme (Q-SORT) [grant number 766970].

Notes on contributors

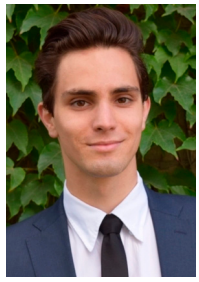

Hugo Larocque is a graduate student in physics at the University of Ottawa. His current research interests center on the applications of structured optical and electron waves in quantum technologies, including the conception and implementation of devices that can generate, manipulate, and detect such waves.

Ido Kaminer is a new faculty member at the Technion Faculty of Electrical Engineering, returning from a postdoc at MIT. He studies the fundamentals of light-matter interactions with novel nanophotonics and 2D materials to develop new concepts for radiation generation in spectral ranges inaccessible by existing technology. In his research, Ido likes to apply beautiful mathematics and algorithmics to solve problems in science and technology and attempts to confront open questions in physics and mathematics. Ido is an Azrieli Faculty Fellow and won a Marie Curie Fellowship for his postdoc, as well as the American Physical Society DLS dissertation award and the Israel Physical Society theory prize for his PhD.

Vincenzo Grillo is a senior researcher at CNR. In the past, he has developed TEM-STEM methods for chemical analysis. His current research concerns vortex beams and holographic beam generation. His research primarily focuses on phase holograms, large vortex beams, and the theory of spin-orbit coupling with electron vortices. In 2016, for his work on structured electron beams, he has received the F. W. Bessel Research Award from the Humboldt foundation.

Gerd Leuchs is a Professor of Physics at the University of Erlangen-Nürnberg, a founding director of the Max Planck Institute for the Science of Light, and a member of the 'Max Planck – University of Ottawa Centre for Extreme and Quantum Photonics'. His specialty lies within the science of light in all of its aspects. He won the Quantum Electronics Prize of the European Physical Society in 2005, the Herbert Walther Award of the OSA and DPG in 2018, and he holds honorary degrees

from the Technical University of Denmark and from St. Petersburg State University. He is a member of the German National Academy of Sciences 'Leopoldina' as well as a foreign member of the Russian Academy of Sciences.

Miles J. Padgett holds the Kelvin Chair of Natural Philosophy at the University of Glasgow. He is fascinated by light both classical and quantum – specifically light's momentum. In 2001 he was elected to Fellowship of the Royal Society of Edinburgh and in 2014 the Royal Society, the UK's National Academy. In 2009, with Les Allen, he won the IoP Young Medal, in 2014 the RSE Kelvin Medal in 2015 the Science of Light Prize from the EPS and in 2017 the Max Born Award of the OSA.

Robert W. Boyd is an internationally recognized leading scientist in nonlinear optics. His research spans a range of topics, from physics to engineering, fundamental to applied research, and classical to quantum nonlinear optics. Boyd became a Canada Excellence Research Chair at the University of Ottawa in 2010. He also holds faculty positions at the University of Rochester in New York and at the University of Glasgow. Most students in optics know his name, as he is the author of Nonlinear Optics, a textbook commonly used around the world.

Mordechai Segev is the Robert J. Shillman Distinguished Professor of Physics, at the Technion. Moti's interests are mainly in nonlinear optics, solitons, sub-wavelength imaging, lasers and quantum electronics. He has won numerous international and national awards, among them the 2007 Quantum Electronics Prize of the European Physics Society, the 2008 Landau Prize, the 2009 Max Born Award of the OSA, and the 2014 Arthur Schawlow Prize of the American Physical Society. In 2011, he was elected to the Israel Academy of Sciences and Humanities, and in 2015 he was elected to the National Academy of Science of the USA. In 2014 Moti Segev won the Israel Prize in Physics.

Ebrahim Karimi holds the Canada Research Chair in the field of structured light at the University of Ottawa. He is also a Visiting Professor at the Max Planck Institute for the Science of Light. His research focuses on experimental and theoretical studies of structured quantum waves, such as photon and electron waves, and their applications in quantum communication, quantum computation, and materials science.

References

[1] Cohen-Tannoudji C, Diu B, Laloe F. Quantum mechanics. Vol. 1. New York (NY): Wiley-VCH; 1986 Jun. p. 626.
[2] Harris J, Grillo V, Mafakheri E, et al. Structured quantum waves. Nat Phys. 2015;11(8):629–634.
[3] McMorran BJ, Agrawal A, Ercius PA, et al. Origins and demonstrations of electrons with orbital angular momentum. Philos Trans R Soc A. 2017;375(2087):20150434.
[4] Bliokh K, Ivanov I, Guzzinati G, et al. Theory and applications of free-electron vortex states. Phys Rep. 2017;690:1–70.
[5] Lloyd S, Babiker M, Thirunavukkarasu G, et al. Electron vortices: beams with orbital angular momentum. Rev Mod Phys. 2017;89(3):035004.
[6] Arfken GB, Weber HJ. Mathematical methods for physicists. 4th ed. Cambridge (MA): Academic Press; 1995.
[7] Grillo V, Karimi E, Gazzadi GC, et al. Generation of nondiffracting electron bessel beams. Phys Rev X. 2014;4(1):011013.
[8] Grillo V, Harris J, Gazzadi GC, et al. Generation and application of bessel beams in electron microscopy. Ultramicroscopy. 2016;166:48–60.
[9] Bliokh KY, Bliokh YP, Savel'ev S, et al. Semiclassical dynamics of electron wave packet states with phase vortices. Phys Rev Lett. 2007;99(19):190404.
[10] Smith S, Leuchs G. Angular correlation in multiphoton ionization of atoms. Adv At Mol Phys. 1988;24:157–221.
[11] Leuchs G, Walther H. Quantum interference effects in field ionization: application to the measurement of the fine structure splitting of highly excited na 2 d states. Z Phys A Hadrons Nucl. 1979;293(2):93–101.
[12] Leuchs G, Smith S, Khawaja E, et al. Quantum beats observed in photoionization. Opt Commun. 1979;31(3):313–316.
[13] Uchida M, Tonomura A. Generation of electron beams carrying orbital angular momentum. Nature. 2010;464(7289):737–739.
[14] Shiloh R, Lereah Y, Lilach Y, et al. Sculpturing the electron wave function using nanoscale phase masks. Ultramicroscopy. 2014;144:26–31.
[15] Verbeeck J, Tian H, Schattschneider P. Production and application of electron vortex beams. Nature. 2010;467(7313):301–304.
[16] Grillo V, Gazzadi GC, Karimi E, et al. Highly efficient electron vortex beams generated by nanofabricated phase holograms. Appl Phys Lett. 2014;104(4):043109.
[17] McMorran BJ, Agrawal A, Anderson IM, et al. Electron vortex beams with high quanta of orbital angular momentum. Science. 2011;331(6014):192–195.
[18] Grillo V, Gazzadi GC, Mafakheri E, et al. Holographic generation of highly twisted electron beams. Phys Rev Lett. 2015;114(3):034801.
[19] Aharonov Y, Bohm D. Significance of electromagnetic potentials in the quantum theory. Phys Rev. 1959;115(3):485–491.
[20] Berry MV. Quantal phase factors accompanying adiabatic changes. Proceedings of the Royal Society of London A: Mathematical, Physical and Engineering Sciences. 1984;392(1802):45–57.

[21] Béché A, Van Boxem R, Van Tendeloo G, et al. Magnetic monopole field exposed by electrons. Nat Phys. 2014;10(1):26–29.
[22] Ohanian HC. What is spin. Am J Phys. 1986;54(6):500–505.
[23] Bliokh KY, Dennis MR, Nori F. Relativistic electron vortex beams: angular momentum and spin-orbit interaction. Phys Rev Lett. 2011;107(17):174802.
[24] Karimi E, Marrucci L, Grillo V, et al. Spin-to-orbital angular momentum conversion and spin-polarization filtering in electron beams. Phys Rev Lett. 2012;108(4):044801.
[25] Karimi E, Grillo V, Boyd RW, et al. Generation of a spin-polarized electron beam by multipole magnetic fields. Ultramicroscopy. 2014;138:22–27.
[26] Grillo V, Marrucci L, Karimi E, et al. Quantum simulation of a spin polarization device in an electron microscope. New J Phys. 2013;15(9):093026.
[27] Saitoh K, Hasegawa Y, Hirakawa K, et al. Measuring the orbital angular momentum of electron vortex beams using a forked grating. Phys Rev Lett. 2013;111(7):074801.
[28] Qassim H, Miatto FM, Torres JP, et al. Limitations to the determination of a Laguerre-Gauss spectrum via projective, phase-flattening measurement. JOSA B. 2014;31(6):A20–A23.
[29] Grillo V, Tavabi AH, Venturi F, et al. Measuring the orbital angular momentum spectrum of an electron beam. Nat Commun. 2017;8:15536.
[30] McMorran BJ, Harvey TR, Lavery MP. Efficient sorting of free electron orbital angular momentum. New J Phys. 2017;19(2):023053.
[31] Larocque H, Bouchard F, Grillo V, et al. Nondestructive measurement of orbital angular momentum for an electron beam. Phys Rev Lett. 2016;117(15):154801.
[32] Bliokh KY, Schattschneider P, Verbeeck J, et al. Electron vortex beams in a magnetic field: a new twist on landau levels and Aharonov-Bohm states. Phys Rev X. 2012;2(4):041011.
[33] Schattschneider P, Schachinger T, Stöger-Pollach M, et al. Imaging the dynamics of free-electron landau states. Nat Commun. 2014;5:4586.
[34] Midgley PA, Dunin-Borkowski RE. Electron tomography and holography in materials science. Nat Mater. 2009;8(4):271–280.
[35] Pozzi G, Hawkes PW. Particles and waves in electron optics and microscopy. Cambridge (MA): Academic Press; 2016.
[36] Hÿtch M, Houdellier F, Hüe F, et al. Nanoscale holographic interferometry for strain measurements in electronic devices. Nature. 2008;453(7198):1086–1089.
[37] Krivanek OL, Lovejoy TC, Dellby N, et al. Vibrational spectroscopy in the electron microscope. Nature. 2014;514(7521):209–212.
[38] Piazza L, Lummen T, Quinonez E, et al. Simultaneous observation of the quantization and the interference pattern of a plasmonic near-field. Nat Commun. 2015;6:6407.
[39] Schattschneider P, Rubino S, Hébert C, et al. Detection of magnetic circular dichroism using a transmission electron microscope. Nature. 2006;441(7092):486–488.
[40] Rusz J, Muto S, Spiegelberg J, et al. Magnetic measurements with atomic-plane resolution. Nat Commun. 2016;7:12672.
[41] Schachinger T, Löffler S, Steiger-Thirsfeld A, et al. Emcd with an electron vortex filter: limitations and possibilities. Ultramicroscopy. 2017;179:15–23.
[42] Lloyd S, Babiker M, Yuan J. Quantized orbital angular momentum transfer and magnetic dichroism in the interaction of electron vortices with matter. Phys Rev Lett. 2012;108(7):074802.
[43] Asenjo-Garcia A, de Abajo FG. Dichroism in the interaction between vortex electron beams, plasmons, and molecules. Phys Rev Lett. 2014;113(6):066102.
[44] Harvey TR, Pierce JS, Chess JJ, et al. Demonstration of electron helical dichroism as a local probe of chirality. 2015, preprint arXiv:150701810.
[45] Xin HL, Zheng H. On-column 2p bound state with topological charge ±1 excited by an atomic-size vortex beam in an aberration-corrected scanning transmission electron microscope. 2012, preprint arXiv:12040021.
[46] Lubk A, Clark L, Guzzinati G, et al. Topological analysis of paraxially scattered electron vortex beams. Phys Rev A. 2013;87(3):033834.
[47] Edström A, Lubk A, Rusz J. Elastic scattering of electron vortex beams in magnetic matter. Phys Rev Lett. 2016;116(12):127203.
[48] Grillo V, Harvey TR, Venturi F, et al. Observation of nanoscale magnetic fields using twisted electron beams. Nat Commun. 2017;8(1):689.
[49] Juchtmans R, Béché A, Abakumov A, et al. Using electron vortex beams to determine chirality of crystals in transmission electron microscopy. Phys Rev B. 2015;91(9):094112.
[50] Verbeeck J, Tian H, Van Tendeloo G. How to manipulate nanoparticles with an electron beam? Adv Mater. 2013;25(8):1114–1117.
[51] Ivanov IP, Karlovets DV. Detecting transition radiation from a magnetic moment. Phys Rev Lett. 2013;110(26):264801.
[52] Berry MV, Balazs NL. Nonspreading wave packets. Am J Phys. 1979;47(3):264–267.
[53] Voloch-Bloch N, Lereah Y, Lilach Y, et al. Generation of electron airy beams. Nature. 2013;494(7437):331–335.
[54] Kaminer I, Nemirovsky J, Rechtsman M, et al. Self-accelerating dirac particles and prolonging the lifetime of relativistic fermions. Nat Phys. 2015;11(3):261–267.
[55] Kaminer I, Bekenstein R, Nemirovsky J, et al. Nondiffracting accelerating wave packets of Maxwell's equations. Phys Rev Lett. 2012;108(16):163901.
[56] Durnin J, Miceli J Jr, Eberly J. Diffraction-free beams. Phys Rev Lett. 1987;58(15):1499–1501.
[57] Allen L, Beijersbergen MW, Spreeuw R, et al. Orbital angular momentum of light and the transformation of Laguerre-Gaussian laser modes. Phys Rev A. 1992;45(11):8185–8189.
[58] Siviloglou G, Broky J, Dogariu A, et al. Observation of accelerating airy beams. Phys Rev Lett. 2007;99(21):213901.
[59] Salandrino A, Christodoulides DN. Airy plasmon: a nondiffracting surface wave. Opt Lett. 2010;35(12):2082–2084.

[60] Liu W, Neshev DN, Shadrivov IV, et al. Plasmonic airy beam manipulation in linear optical potentials. Opt Lett. 2011;36(7):1164–1166.
[61] Zhang P, Wang S, Liu Y, et al. Plasmonic airy beams with dynamically controlled trajectories. Opt Lett. 2011;36(16):3191–3193.
[62] Li L, Li T, Wang S, et al. Plasmonic airy beam generated by in-plane diffraction. Phys Rev Lett. 2011;107(12):126804.
[63] Minovich A, Klein AE, Janunts N, et al. Generation and near-field imaging of airy surface plasmons. Phys Rev Lett. 2011;107(11):116802.
[64] Epstein I, Arie A. Arbitrary bending plasmonic light waves. Phys Rev Lett. 2014;112(2):023903.
[65] Libster-Hershko A, Epstein I, Arie A. Rapidly accelerating mathieu and weber surface plasmon beams. Phys Rev Lett. 2014;113(12):123902.
[66] Zhang P, Li T, Zhu J, et al. Generation of acoustic self-bending and bottle beams by phase engineering. Nat Commun. 2014;5:4316.
[67] Bar-Ziv U, Postan A, Segev M. Observation of shape-preserving accelerating underwater acoustic beams. Phys Rev B. 2015;92(10):100301.
[68] Fu S, Tsur Y, Zhou J, et al. Propagation dynamics of airy water-wave pulses. Phys Rev Lett. 2015;115(3):034501.
[69] Peleg O, Bartal G, Freedman B, et al. Conical diffraction and gap solitons in honeycomb photonic lattices. Phys Rev Lett. 2007;98(10):103901.
[70] Jacob Z, Alekseyev LV, Narimanov E. Optical hyperlens: far-field imaging beyond the diffraction limit. Opt Express. 2006;14(18):8247–8256.
[71] Bialynicki-Birula I, Bialynicka-Birula Z. Relativistic electron wave packets carrying angular momentum. Phys Rev Lett. 2017;118:114801.
[72] Barnett SM. Relativistic electron vortices. Phys Rev Lett. 2017;118:114802.
[73] Bliokh KY, Dennis MR, Nori F. Position, spin, and orbital angular momentum of a relativistic electron. Phys Rev A. 2017 Aug;96:023622.
[74] Larocque H, Karimi E. Viewpoint: a new twist on relativistic electron vortices. Physics. 2017;10:26.